



EDGEWOOD CHEMICAL BIOLOGICAL CENTER

U.S. ARMY RESEARCH, DEVELOPMENT AND ENGINEERING COMMAND
Aberdeen Proving Ground, MD 21010-5424

ECBC-TR-1428

COMPUTER CODE FOR INTERPRETING ^{13}C NMR RELAXATION MEASUREMENTS WITH SPECIFIC MODELS OF MOLECULAR MOTION: THE RIGID ISOTROPIC AND SYMMETRIC TOP ROTOR MODELS AND THE FLEXIBLE SYMMETRIC TOP ROTOR MODEL

Terry J. Henderson

RESEARCH AND TECHNOLOGY DIRECTORATE

January 2017

Approved for public release; distribution unlimited.



Disclaimer

The findings in this report are not to be construed as an official Department of the Army position unless so designated by other authorizing documents.

REPORT DOCUMENTATION PAGE

Form Approved
OMB No. 0704-0188

Public reporting burden for this collection of information is estimated to average 1 h per response, including the time for reviewing instructions, searching existing data sources, gathering and maintaining the data needed, and completing and reviewing this collection of information. Send comments regarding this burden estimate or any other aspect of this collection of information, including suggestions for reducing this burden to Department of Defense, Washington Headquarters Services, Directorate for Information Operations and Reports (0704-0188), 1215 Jefferson Davis Highway, Suite 1204, Arlington, VA 22202-4302. Respondents should be aware that notwithstanding any other provision of law, no person shall be subject to any penalty for failing to comply with a collection of information if it does not display a currently valid OMB control number. **PLEASE DO NOT RETURN YOUR FORM TO THE ABOVE ADDRESS.**

1. REPORT DATE (DD-MM-YYYY) XX-01-2017		2. REPORT TYPE Final		3. DATES COVERED (From - To) Oct 2013 – Jun 2016	
4. TITLE AND SUBTITLE Computer Code for Interpreting ¹³ C NMR Relaxation Measurements with Specific Models of Molecular Motion: The Rigid Isotropic and Symmetric Top Rotor Models and the Flexible Symmetric Top Rotor Model				5a. CONTRACT NUMBER	
				5b. GRANT NUMBER	
				5c. PROGRAM ELEMENT NUMBER	
6. AUTHOR(S) Henderson, Terry J.				5d. PROJECT NUMBER CB3889	
				5e. TASK NUMBER	
				5f. WORK UNIT NUMBER	
7. PERFORMING ORGANIZATION NAME(S) AND ADDRESS(ES) Director, ECBC, ATTN: RDCB-DRC-C, APG, MD 21010-5424				8. PERFORMING ORGANIZATION REPORT NUMBER ECBC-TR-1428	
9. SPONSORING / MONITORING AGENCY NAME(S) AND ADDRESS(ES) Defense Threat Reduction Agency, 8725 John J. Kingman Road, MSC 6201, Fort Belvoir, VA 22060-6201				10. SPONSOR/MONITOR'S ACRONYM(S) DTRA	
				11. SPONSOR/MONITOR'S REPORT NUMBER(S)	
12. DISTRIBUTION / AVAILABILITY STATEMENT Approved for public release; distribution unlimited.					
13. SUPPLEMENTARY NOTES					
14. ABSTRACT: Carbon-13 nuclear magnetic resonance (¹³ C NMR) spectroscopy is a powerful technique for investigating the motional behavior of molecules in solution. Such investigations commonly include the interpretation of ¹³ C relaxation measurements with specific models of molecular motion. This report describes the fundamental theory and selected results from mathematical modeling programs for three such models, the rigid isotropic and rigid symmetric top rotor models and the flexible symmetric top rotor model, which all have been adopted for interpreting ¹³ C NMR spin-lattice relaxation time (<i>T</i> ₁), spin-spin relaxation time (<i>T</i> ₂), and nuclear Overhauser enhancement factor (η_c) measurements. The results for the rigid isotropic rotor illustrate the general behavior of <i>T</i> ₁ , <i>T</i> ₂ , and η_c as a function of rotational correlation time (τ_c). Results for different magnetic field strengths are included to show the dependence of the relaxation values on field strength. The symmetric top rotor results illustrate how the model's two correlation times and the orientational dependence of the ¹³ C- ¹ H relaxation vector with the symmetric top major axis affect relaxation behavior. Finally, the results of the flexible symmetric top rotor model are presented to reveal how progressively adding internal motion into a symmetric top rotor molecule diminishes this orientational dependence.					
15. SUBJECT TERMS Isotropic rotor Nuclear magnetic resonance (NMR) Spectral density functions Spin-spin relaxation Molecular dynamics Nuclear Overhauser effect Symmetric top rotor Spin-lattice relaxation					
16. SECURITY CLASSIFICATION OF:			17. LIMITATION OF ABSTRACT	18. NUMBER OF PAGES	19a. NAME OF RESPONSIBLE PERSON
a. REPORT	b. ABSTRACT	c. THIS PAGE			Renu B. Rastogi
U	U	U	UU	38	19b. TELEPHONE NUMBER (include area code) (410) 436-7545

Blank

PREFACE

The work described in this report was authorized under project no. CB3889. The work was started in October 2013 and completed in June 2016.

The use of either trade or manufacturers' names in this report does not constitute an official endorsement of any commercial products. This report may not be cited for purposes of advertisement.

This report has been approved for public release.

Blank

CONTENTS

1.	INTRODUCTION	1
2.	THEORY	2
2.1	Principles of ^{13}C Relaxation.....	3
2.2	Spectral Density Functions	4
3.	COMPUTER CODE DEVELOPMENT	6
4.	RESULTS	6
4.1	The Rigid Isotropic Rotor Model.....	6
4.2	The Rigid Symmetric Top Rotor Model.....	9
4.2.1	Results of Varying β	9
4.2.2	Results from Varying τ_z/τ_x	11
4.3	The Flexible Symmetric Top Rotor Model.....	13
5.	DISCUSSION AND CONCLUSIONS	14
	LITERATURE CITED	15
	ACRONYMS AND ABBREVIATIONS	17
	APPENDIX: MLAB CODE USED TO GENERATE FIGURES 2 THROUGH 8	19

FIGURES

1.	Models of overall molecular rotational reorientation	2
2.	Rigid isotropic rotor T_1 as a function of τ_c	7
3.	Rigid isotropic rotor T_2 as a function of τ_c	8
4.	Rigid isotropic rotor η_C (NOEF) as a function of τ_c	9
5.	Changes in symmetric top rotor T_1 induced by varying β	10
6.	Rigid symmetric top rotor T_1 as a function of τ_x for different values of τ_z/τ_x	12
7.	Rigid symmetric top rotor η_C (NOEF) as a function of τ_x for different values of τ_z/τ_x	12
8.	The diminishing dependence on β induced by increasing internal motion	13

COMPUTER CODE FOR INTERPRETING ^{13}C NMR RELAXATION MEASUREMENTS WITH SPECIFIC MODELS OF MOLECULAR MOTION: THE RIGID ISOTROPIC AND SYMMETRIC TOP ROTOR MODELS AND THE FLEXIBLE SYMMETRIC TOP ROTOR MODEL

1. INTRODUCTION

Nuclear magnetic resonance (NMR) spectroscopy is a tremendously powerful technique for analyzing the structure, conformation, and architecture of molecules and molecular systems. Both one- and two-dimensional methods have provided valuable information for molecules ranging in size from the simplest solvent molecules to extremely large protein complexes. Another valuable application of NMR spectroscopy concerns the property of molecular motion, which is related to many physical, and even biological, functions of molecules in solution. Investigating the motional dynamics of molecular systems provides not only complementary information about structure and conformation, but also a deeper insight into the physical behavior of the molecules in general and the biological properties of molecules from living systems.

NMR spectroscopy has long been exploited to evaluate molecular motions, and has been extensively applied to dynamic problems for many different types of molecules and molecular complexes (Lyerla and Levy, 1974; Heatley, 1979). In particular, carbon-13 nuclear magnetic resonance (^{13}C NMR) relaxation measurements can be used to simultaneously evaluate motion at several different carbon sites on a molecule's framework. The NMR signal of each carbon nucleus is associated with a set of relaxation parameters that reflect the average interaction of that nucleus with the environment. Such ^{13}C relaxation parameters, including the spin-lattice relaxation time (T_1), spin-spin relaxation time (T_2), and the nuclear Overhauser effect (NOE), are related to the spectral density, or power spectrum, of local magnetic fields that are generated by the atomic and electronic environment of the nucleus. Modulated by the overall molecular rotational reorientation, or the tumbling of the molecule in solution, together with its internal motions (motions involving parts of the molecule such as rotations of methyl groups), these local fields can promote relaxation when they have a frequency component at or near the Larmor frequency of the nucleus. This provides a direct link between nuclear magnetic relaxation and molecular motion.

The persistence of the fluctuating local fields before they are averaged to zero by molecular motion, and hence their effectiveness in producing relaxation, is described by a time-correlation function. Because this function embodies all of the information about the mechanisms and rates of motion for molecules, obtaining it is the crucial point for a quantitative interpretation of relaxation data. As described herein, the spectral-density and time-correlation functions are Fourier transform pairs that interrelate motional frequencies (the spectral density function and frequency domain) and motional rates (the time-correlation function and time domain). In the simplest case, the tumbling of a rigid (no internal motions) molecule is described by a single correlation time. This is the *rigid isotropic rotor model*, which is used to describe the molecular tumbling of highly symmetrical molecules such as methane or fullerenes (buckyballs).

A second model used for rigid molecules is based on the rotational reorientation of a prolate ellipsoid (Woessner, 1962). These ellipsoids are often used as an approximation to symmetric top molecules such as a helix, and the feasibility and reasonableness of this practice has been discussed elsewhere (Torchia et al., 1975; Schleich et al., 1989). This *rigid symmetric top rotor model* includes two correlation times for describing molecular rotational reorientation about the ellipsoid minor and major axes. In addition, the model can be modified to include the effects of internal motions, giving a third model, the *flexible symmetric top rotor model*, used to represent flexible helical structures such as DNA fragments (Withka et al., 1991). This report reviews the fundamental theory and selected mathematical results that were created to model T_1 , T_2 , and NOE measurements in terms of the three models of overall molecular rotational reorientation. All three models are illustrated in Figure 1.

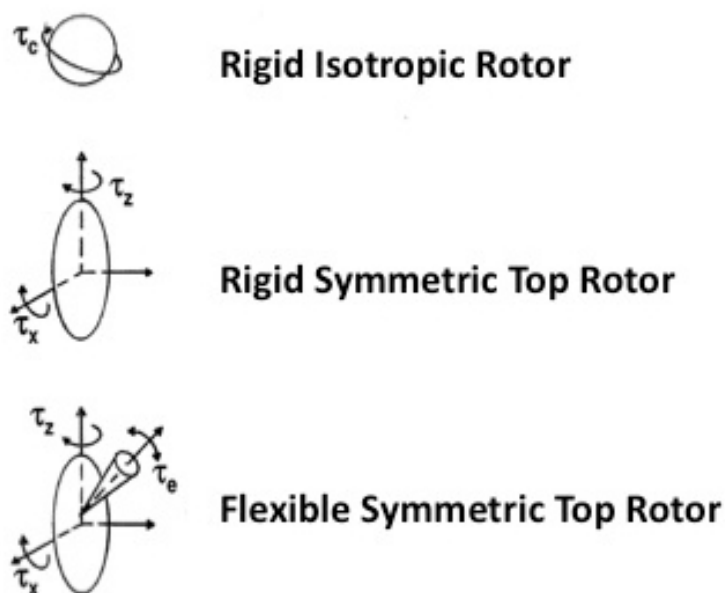


Figure 1. Models of overall molecular rotational reorientation. τ_c is the correlation time describing the molecular tumbling of an isotropic rotor. The model is commonly used for highly symmetric, small molecules and for symmetric globular proteins. τ_x and τ_z are the correlation times for molecular tumbling about the minor (x) and major (z) axes, respectively, of a symmetric top rotor, which is represented as a prolate ellipsoid. The model is typically used for molecular helices such as small fragments of DNA and α -helices. The flexible symmetric top rotor superimposes an effective correlation time, τ_e , onto a symmetric top rotor to account for internal motion.

2. THEORY

The purpose of this section is to outline some fundamental aspects as a framework for discussing the quantitative features of nuclear magnetic relaxation and to specifically describe how simple ^{13}C relaxation theory is used to describe quantitatively simple molecular

motions. More-detailed accounts of nuclear magnetic relaxation can be found in a number of basic textbooks (i.e., Farrar and Becker, 1971; Fukushima and Roeder, 1981; Harris, 1986).

2.1 Principles of ^{13}C Relaxation

Magnetic relaxation arises from fluctuating terms in the spin Hamiltonian. By far, the most-important term for organic molecules is the intramolecular dipole–dipole interaction, which is time-dependent because of molecular rotation. The relaxation times of ^{13}C nuclei in $^{13}\text{CH}_n$ groups ($n > 0$) are dominated by the dipolar interactions with their attached protons, with very few exceptions (Heatley, 1979). Because the ^{13}C – ^1H bond length remains constant to a high degree of accuracy from one organic molecule to another, ^{13}C relaxation times are a reliable probe for molecular mobility. ^{13}C relaxation times are normally measured with full proton decoupling, and under this condition, the T_1 and T_2 values for a ^{13}C nucleus in a $^{13}\text{CH}_n$ group that is relaxed solely by interaction with the attached protons is given by (Doddrell et al., 1972)

$$\frac{1}{T_1} = \frac{1}{20} \left(\frac{\mu_0}{4\pi} \right)^2 \frac{\gamma_{\text{H}}^2 \gamma_{\text{C}}^2 \hbar^2}{r_{\text{CH}}^6} \{ J(\omega_{\text{H}} - \omega_{\text{C}}) + 3J(\omega_{\text{C}}) + 6J(\omega_{\text{H}} + \omega_{\text{C}}) \} \quad (1)$$

and

$$\frac{1}{T_2} = \frac{1}{40} \left(\frac{\mu_0}{4\pi} \right)^2 \frac{\gamma_{\text{H}}^2 \gamma_{\text{C}}^2 \hbar^2}{r_{\text{CH}}^6} \{ 4J(0) + J(\omega_{\text{H}} - \omega_{\text{C}}) + 3J(\omega_{\text{C}}) + 6J(\omega_{\text{H}}) + 6J(\omega_{\text{H}} + \omega_{\text{C}}) \} \quad (2)$$

where γ_{H} and γ_{C} are the nuclear magnetogyric ratios for protons and ^{13}C nuclei, respectively; ω_{H} and ω_{C} are the resonance frequencies for protons and ^{13}C nuclei, respectively; μ_0 is the permeability of free space ($4\pi \times 10^{-7} \text{ Hm}^{-1}$); and r_{CH} is the internuclear distance (assumed to be a constant 1.09 \AA). The $J(\omega)$ terms are the spectral density functions for specific frequencies, which are described in Section 2.2.

Irradiation of the protons gives rise to an enhancement of the integrated ^{13}C signal intensity due to a ^{13}C – ^1H NOE (Doddrell et al., 1972). If the protons are completely saturated, the NOE enhancement factor, commonly designated as NOEF or η_{C} , is given by

$$\eta_{\text{C}} = \frac{S^{\text{d}} - S^0}{S^0} = \frac{\gamma_{\text{H}}}{\gamma_{\text{C}}} \left\{ \frac{6J(\omega_{\text{H}} + \omega_{\text{C}}) - J(\omega_{\text{H}} - \omega_{\text{C}})}{J(\omega_{\text{H}} - \omega_{\text{C}}) + 3J(\omega_{\text{C}}) + 6J(\omega_{\text{H}} + \omega_{\text{C}})} \right\} \quad (3)$$

where S^{d} and S^0 are the ^{13}C integrated intensities with and without proton irradiation, respectively. Some investigators report NOE values directly rather than η_{C} , which are related by

$$\text{NOE} = \frac{S^{\text{d}}}{S^0} = 1 + \eta_{\text{C}} \quad (4)$$

2.2 Spectral Density Functions

For any one value of ω , $J_n(\omega)$ is defined by

$$J_n(\omega) = \int_{-\infty}^{+\infty} G_n(\tau) e^{-i\omega\tau} d\tau \quad (5)$$

where $G_n(\tau)$ is the autocorrelation function for all time-dependent motional events contributing to the reorientation of the $^{13}\text{C}-^1\text{H}$ bond vector in a laboratory-fixed frame

$$G_n(\tau) = \langle F_n^*(t + \tau) F_n(t) \rangle \quad (6)$$

The equation states that $G_n(\tau)$ is the ensemble average (conformational average) of all $^{13}\text{C}-^1\text{H}$ dipole-dipole interactions contributing to the relaxation of the ^{13}C signal. Each interaction is defined in terms of a space function evaluated at time t , and later time $t + \tau$; these are designated as $F_n(t)$ and $F_n(t + \tau)$ in the equation, respectively. The asterisk in the $F_n(t + \tau)$ term designates that its value may include contributions from magnetic field strength inhomogeneities in addition to those from relaxation. The space functions include an angle ρ that relates the orientation of the $^{13}\text{C}-^1\text{H}$ bond vector to that of the NMR spectrometer static magnetic field (the z axis of a Cartesian coordinate system fixed in the laboratory frame). There is a single space function for each dimension in three-dimensional space:

$$\begin{aligned} F_0(t) &= \left(\frac{5}{4}\right)^{1/2} [1 - 3 \cos^2 \rho(t)] \\ F_1(t) &= \left(\frac{15}{4}\right)^{1/2} [\sin \rho(t) \cos \theta(t) \exp(i\phi(t))] \\ F_2(t) &= \left(\frac{15}{8}\right)^{1/2} [\sin^2 \rho(t) \exp(2i\phi(t))] \end{aligned}$$

In addition, when the value of r_{CH} is time-dependent, it should be included in a refined definition of $G_n(t)$. When a rigid molecule reorients by isotropic rotational diffusion (see Figure 1), $G_n(t)$ is exponential

$$G_n(t) = \overline{|F_n(t)|^2} \exp\left(-\frac{|t|}{\tau_c}\right) = \exp\left(-\frac{|t|}{\tau_c}\right) \quad (7)$$

because the quantities $F_n(t)$ are defined to give the unit mean square. Therefore, the subscript n on $J_n(\omega)$ is dropped henceforth, and $J(\omega)$ takes the familiar form

$$J(\omega) = \frac{2\tau_c}{1 + \omega^2 \tau_c^2} \quad (8)$$

Woessner (1962) derived the $J(\omega)$ for anisotropic rotational reorientation in a manner parallel to that described for the isotropic case. Full anisotropic reorientation assumes that rotational reorientation about each of the orthogonal axes in three-dimensional space (the x , y , and z axes) is unique and therefore is represented by three unique correlation times. The symmetric top rotor is a special case of this model where the molecular tumbling about two of the three axes is identical (degenerate), and both can be represented by a single correlation time to give a total of two unique correlation times (τ_x and τ_z in Figure 1). The identical tumbling rates can arise from molecular symmetry, which is why the model is used for helical molecules. The $J(\omega)$ for a rigid symmetric top rotor can be derived by replacing τ_c in eq 8 with an effective correlation time that relates the $^{13}\text{C}-^1\text{H}$ relaxation vector to the major axis (τ_z) with an angle, β . Expressed in terms of τ_x and τ_z , $J(\omega)$ takes the following form:

$$\begin{aligned}
 J(\omega) = & 12\tau_x \left\{ \frac{\left(\frac{1}{4}\right)(3\cos^2\beta - 1)^2}{6} + \frac{\left(\frac{3}{4}\right)\sin^2(2\beta)}{5 + \frac{\tau_x}{\tau_z}} \right. \\
 & \left. + \frac{\left(\frac{3}{4}\right)\sin^4\beta}{2 + 4\left(\frac{\tau_x}{\tau_z}\right)} \right\} \Bigg/ \left[1 + \omega^2 \left[12\tau_x \left\{ \frac{\left(\frac{1}{4}\right)(3\cos^2\beta - 1)^2}{6} \right. \right. \right. \\
 & \left. \left. \left. + \frac{\left(\frac{3}{4}\right)\sin^2(2\beta)}{5 + \frac{\tau_x}{\tau_z}} + \frac{\left(\frac{3}{4}\right)\sin^4\beta}{2 + 4\left(\frac{\tau_x}{\tau_z}\right)} \right\} \right] \right] \quad (9)
 \end{aligned}$$

In cases where $\tau_x = \tau_z$, the equation reduces to the isotropic rotor $J(\omega)$ shown in eq 8, regardless of the value for β .

Equation 8 can also be modified to include the effects of internal motion for a symmetric top rotor by substituting τ_c with a different effective correlation time, designated herein as τ_e . Described by Withka and coworkers (1991), τ_e not only relates the $^{13}\text{C}-^1\text{H}$ relaxation vector to τ_z with β , but also relates the internal diffusion of the $^{13}\text{C}-^1\text{H}$ relaxation vector within an ellipsoid cone (refer to the symmetric top rotor with internal motions model in Figure 1). The expression for τ_e is

$$\begin{aligned}
 \tau_e = & \frac{\frac{1}{4} + \frac{9}{8\exp(4\theta^2)} + \frac{3\cos(2\beta)}{2\exp(2\theta^2)} + \frac{9\cos(4\beta)}{8\exp(4\theta^2)}}{4\tau_x} \\
 & + \frac{9 \left\{ 1 + \frac{1}{2\exp(4\theta^2)} - \frac{2\cos(2\beta)}{\exp(2\theta^2)} + \frac{\cos(4\beta)\exp(-4\theta^2 - 4\varepsilon^2)}{2} \right\}}{16(\tau_x^{-1} + 2\tau_z^{-1})} \\
 & + \frac{9 \{ \exp(-4\theta^2) - \exp(-4\theta^2 - \varepsilon^2) \cos(4\beta) \}}{4(5\tau_x^{-1} + \tau_z^{-1})} \quad (10)
 \end{aligned}$$

In the equation, θ is the square root of the mean square polar angle of motion, and ε is the square root of the mean square azimuthal angle of motion. In the absence of internal motions ($\theta = \varepsilon = 0^\circ$), the expression that is derived from substituting τ_c in eq 8 with τ_e reduces to the symmetric top rotor $J(\omega)$ in eq 9.

3. COMPUTER CODE DEVELOPMENT

The software program MLAB (Civilized Software, Inc.; Silver Spring, MD) was used to create mathematical modeling programs to plot T_1 , T_2 , and η_C values as a function of correlation time for the rigid isotropic and symmetric top rotor models and for the flexible symmetric top rotor model. Magnetic field strengths of 11.75, 16.45, 18.8, and 21.5 T (Tesla; ^1H Larmor frequencies of 500, 700, 800, and 900 MHz, respectively) were used exclusively, as these are commercially available field strengths that are typically found in ^{13}C nuclear magnetic relaxation investigations. The effects of varying β in both symmetric top rotor models were also evaluated in detail. In every case, the computer code was rigorously tested to ensure that their results returned the relaxation behavior described in textbooks and the scientific literature. For all calculations, a value of 1.09 Å was used for r_{CH} . Appendix A contains the computer code used to generate Figures 2–8.

4. RESULTS

The results for the rigid isotropic rotor are presented to illustrate the general behavior of T_1 , T_2 , and η_C as a function of τ_c . Calculated data for different magnetic field strengths are included to illustrate the field strength dependence of nuclear magnetic relaxation. The rigid symmetric top rotor results are then presented to show how parameters specific to the model affect relaxation behavior. Data calculated for this model also include rigid isotropic rotor data that are provided strictly for comparison, and only a single magnetic field strength is shown to ensure that the figures are clearly presented. The results from the flexible symmetric top rotor model are presented last, in a manner revealing how progressively adding internal motion into a symmetric top rotor affects τ_c values.

4.1 The Rigid Isotropic Rotor Model

Figure 2 shows rigid isotropic rotor T_1 values as a function of τ_c , which was calculated at magnetic field strengths of 16.45, 18.80, and 21.15 T. The corresponding T_2 and η_C results are shown in Figures 3 and 4, respectively. As these relaxation times and η_C values are frequency-dependent quantities (see eqs 1–3), their behaviors are closely related to the relative magnitudes of ω and τ_c in eq 8. For rapid motions ($\omega \ll 1/\tau_c$), eq 8 becomes

$$J(\omega) = \langle F^2(0) \rangle 2\tau_c \quad (11)$$

and T_1 , T_2 , and η_C are all quantities that are not dependent on magnetic field strength, which decreases continually as τ_c increases (motions become slower). This field strength independence for both relaxation times, and their continual decrease associated with increasing τ_c , are clearly shown in Figures 2 and 3 for $\tau_c \leq 10^{-11}$ s. In this region of fast motions, which is the so-called extreme narrowing limit, eqs 1–3 simplify to

$$\frac{1}{T_1} = \frac{1}{T_2} = \frac{\gamma_H^2 \gamma_C^2 \hbar^2}{r_{CH}^6} \tau_c \quad (12)$$

and

$$\eta_C = \frac{S^d - S^0}{S^0} = \frac{\gamma_H}{2\gamma_C} = 1.988 \quad (13)$$

Equation 12 indicates that $T_1 = T_2$ in this region, which can be seen by comparing Figures 2 and 3, while eq 13 shows that η_C also attains its maximum value of 1.988 in this region, which is determined directly by the magnetogyric ratios γ_H and γ_C . The latter point is illustrated in Figure 4, where the η_C values for all three magnetic field strengths reach this maximum value at $\tau_c = 10^{-11}$ s.

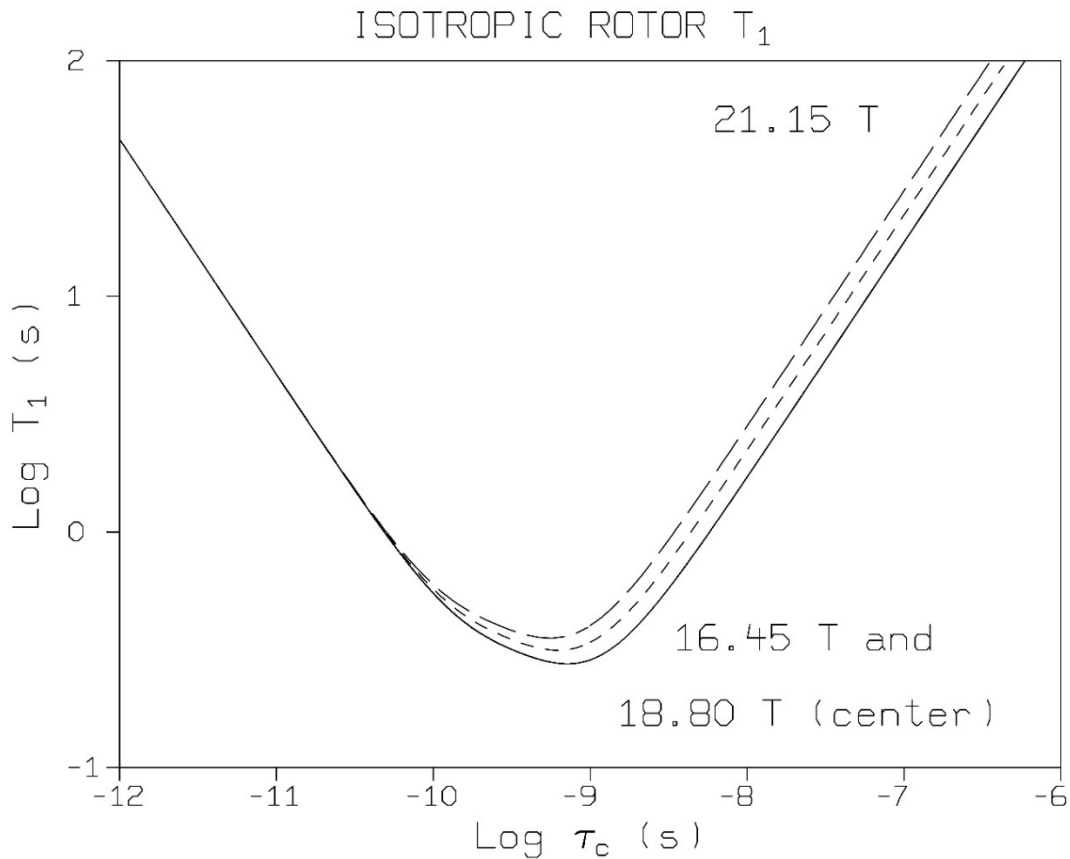


Figure 2. Rigid isotropic rotor T_1 as a function of τ_c . Results are shown for magnetic field strengths of 16.45, 18.80, and 21.15 T.

At a Larmor frequency of $\omega \approx 1/\tau_c$; relaxation is the most effective; $J(\omega)$ attains its maximum value; and as shown in Figure 2, T_1 values reach a minimum. For longer correlation times ($\omega > 1/\tau_c$) outside the extreme narrowing limit, relaxation again becomes less effective, and T_1 values increase and become frequency-dependent quantities. This frequency dependence is shown in Figure 2 starting at $\tau_c \approx 10^{-11}$ s and continues as motion slows. T_2 also becomes frequency-dependent at long τ_c , but unlike T_1 , T_2 decreases continually with τ_c to the limit where motion is considered frozen (Figure 3). This behavior is due to the zero frequency-dependence of T_2 (compare eqs 1 and 2) arising from fluctuations in the local fields along the z direction, which is equivalent in the laboratory-fixed frame and molecular system of coordinates. Furthermore, and as shown in Figure 4, η_C also decreases progressively to lower values as motion slows and asymptotically reaches a minimum value of 0.15 for a long τ_c . Therefore, η_C can have values much less than 1.988, despite the fact that dipole-dipole interaction is the dominant relaxation mechanism. The three magnetic field strengths in the figure reveal that η_C can also be a frequency-dependent parameter outside of the extreme narrowing limit. Figure 4 shows that as field strength increases, η_C values concomitantly decrease in this region.

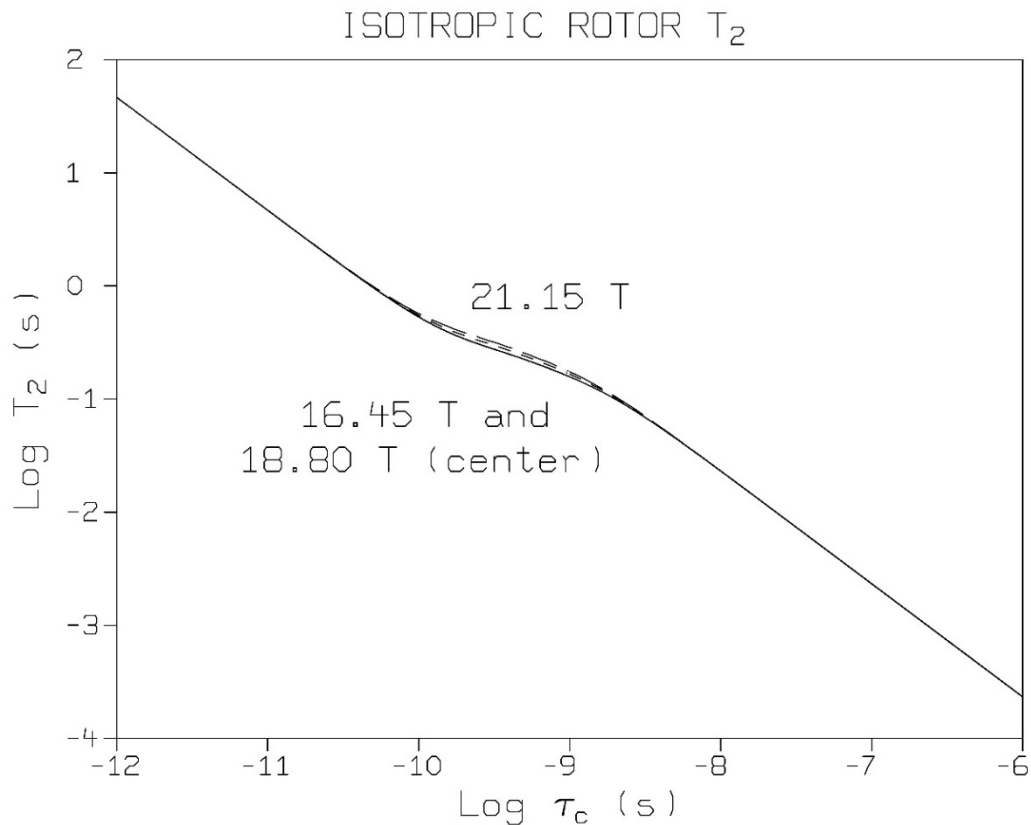


Figure 3. Rigid isotropic rotor T_2 as a function of τ_c . Results are shown for magnetic field strengths of 16.45, 18.80, and 21.15 T.

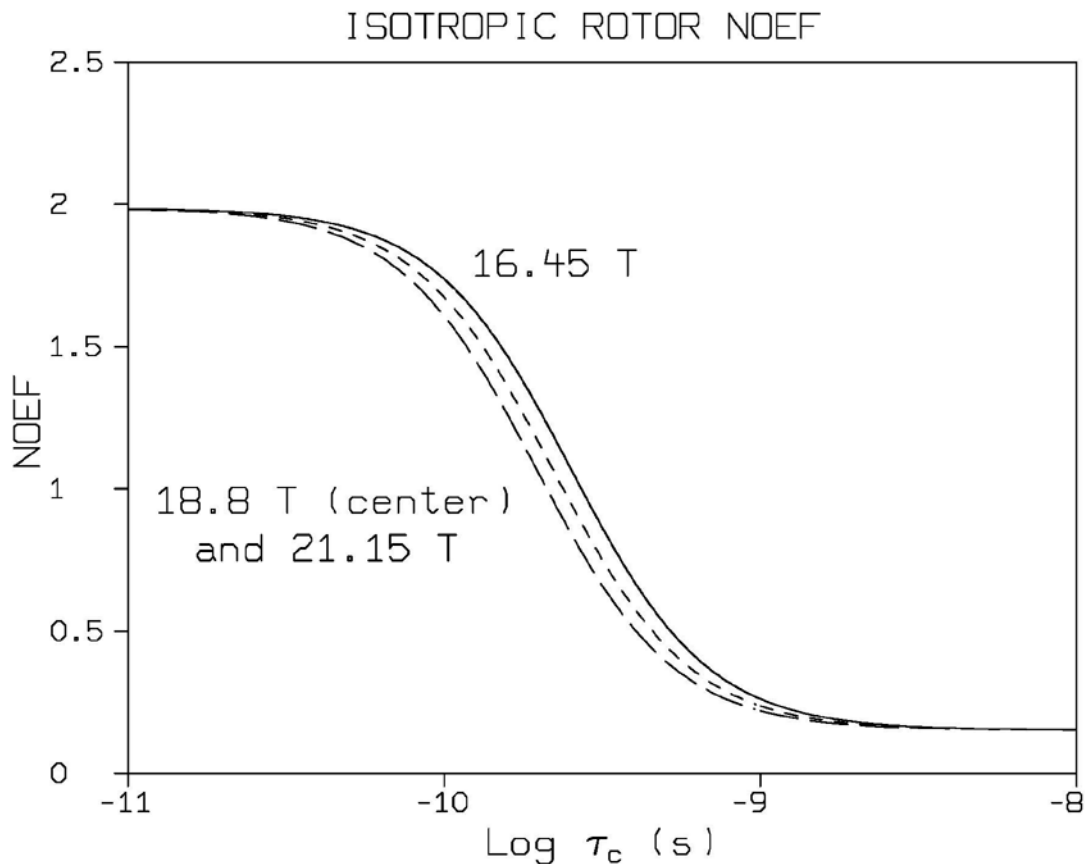


Figure 4. Rigid isotropic rotor η_C (NOEF) as a function of τ_c . Results are shown for magnetic field strengths of 16.45, 18.80, and 21.15 T.

4.2 The Rigid Symmetric Top Rotor Model

In contrast with the isotropic rotor model, the symmetric top rotor model contains three parameters, τ_x , τ_z , and β . A large number of plots can be generated by varying one or more of these parameters to illustrate their theoretical effects on nuclear magnetic relaxation. For simplicity, however, figures displaying symmetric top rotor calculations are presented to illustrate how varying a single parameter of the model theoretically affects T_1 or η_C and returns the model to the isotropic rotor model.

4.2.1 Results of Varying β

Figure 5 illustrates the influence of varying β for a rigid symmetric top rotor on T_1 values. It is of particular interest to consider the $\beta = 0^\circ$ curve because this angle orients the $^{13}\text{C}-^1\text{H}$ relaxation vector parallel to the ellipsoid long axis, where it is not reoriented by rotation about the axis. The curve, therefore, corresponds to the isotropic reorientation of the $^{13}\text{C}-^1\text{H}$ vector by only τ_x . When $\beta > 0^\circ$, the contributions of both τ_x and τ_z to $J(\omega)$ change concomitantly, and T_1 values change in response. As β increases from 0° , the τ_z contribution to

$J(\omega)$ gradually increases until it reaches a maximum at 90° . At the same time, the corresponding τ_x contribution gradually decreases to a minimum at this same β value. Because the T_1 curves were calculated with $\tau_x > \tau_z$, the overall apparent effect is the same as that of increasing the molecular weight or decreasing the temperature. As is shown in Figure 5, this results in T_1 values that concomitantly increase for $\tau_x < 1/\omega$ (the extreme narrowing region) and decrease for larger values of τ_x , as β increases from 0 to 90° . Graphically, the entire T_1 curve for $\beta = 0^\circ$ appears to be displaced horizontally toward longer τ_x values (slower rotation) as β approaches 90° . As expected, the $\beta = 0^\circ$ curves for the corresponding T_2 and η_C calculations also appear to be displaced toward longer τ_x values as β increases from 0 to 90° (not shown). Collectively, these results demonstrate that there can be a strong dependence on β for relaxation times and η_C values. It is clear from Figure 5 that the curves can provide a reliable estimate of T_1 only if the value of β for a $^{13}\text{C}-^1\text{H}$ vector is accurately known.

SYMMETRIC TOP ROTOR T_1 FOR VARIOUS β -ANGLES

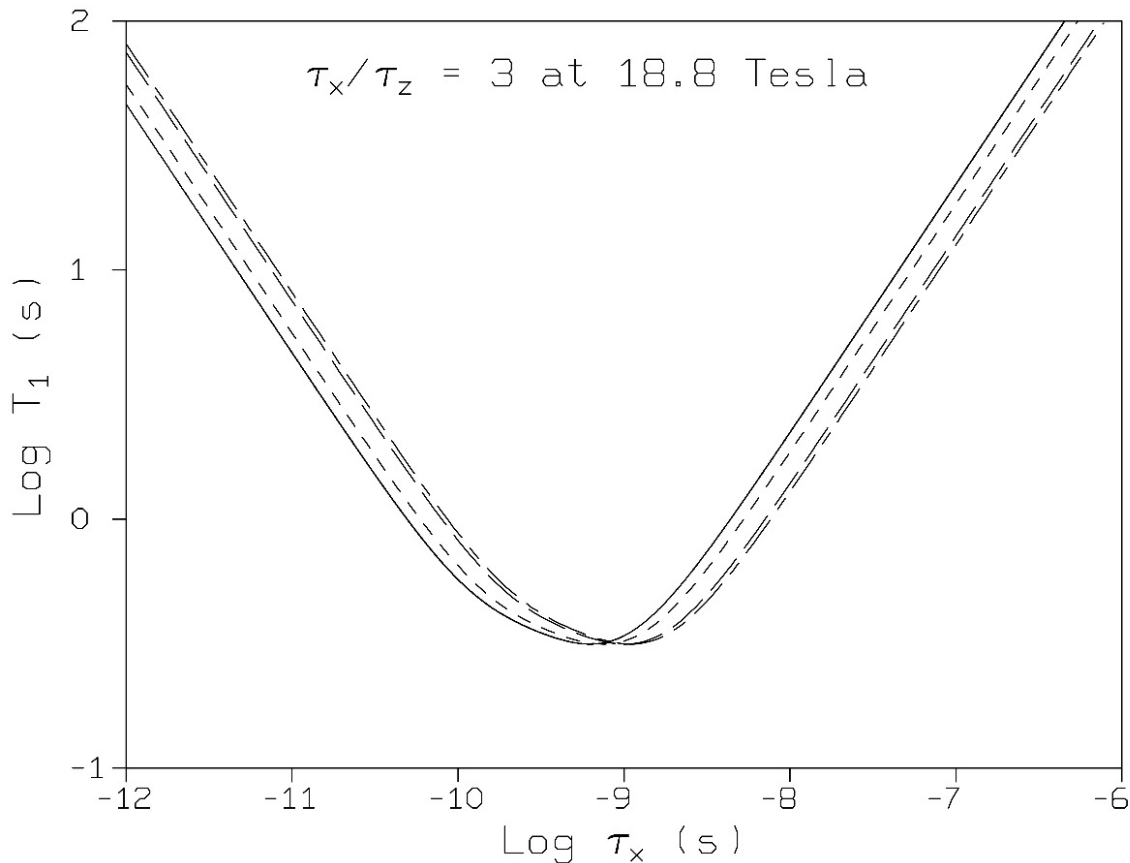


Figure 5. Changes in symmetric top rotor T_1 induced by varying β . Rigid symmetric top rotor T_1 values are plotted as a function of τ_x , as calculated for $\beta = 0^\circ$ (—), 30° (----), 60° (— — —), and 90° (- - - -). All values were calculated with τ_x three times larger than τ_z at a magnetic field strength of 18.80 T.

For the interpretation of NMR relaxation results with the symmetric top rotor model, β values are measured from an assumed or established conformation of the molecule under investigation and can have values between 0 and 180°. As the angles increase from 90°, the τ_z contribution to $J(\omega)$ begins to gradually decrease until $\beta = 180^\circ$, where the $^{13}\text{C}-^1\text{H}$ relaxation vector is once again parallel to the ellipsoid long axis (as in the case of $\beta = 0^\circ$), and τ_z no longer contributes to $J(\omega)$. In concomitant fashion, the τ_x contribution to $J(\omega)$ gradually increases to a maximum at $\beta = 180^\circ$. At this point, the symmetric top model returns the isotropic model with the reorientation of the $^{13}\text{C}-^1\text{H}$ vector, which is described once again by only τ_x . This is the opposite behavior from that described previously for β that increase from 0 to 90°, and this is reflected in the theoretical relaxation times and η_{C} values. For example, as β increases from 90°, the $\beta = 90^\circ$ curve in Figure 5 appears to be displaced back toward shorter τ_x values (faster reorientation) until $\beta = 180^\circ$, where the curve returns to and superimposes with the $\beta = 0^\circ$ curve. Therefore, although Figure 5 only shows data for $0^\circ \leq \beta \leq 90^\circ$, the full range of T_1 behavior for $0^\circ \leq \beta \leq 180^\circ$ is represented in the figure. As expected, the analogous symmetric top rotor T_2 and η_{C} curves for $\beta = 90^\circ$ also appear to be horizontally displaced in a similar manner toward shorter τ_x values as β increases from 90° (not shown).

4.2.2 Results from Varying τ_z/τ_x

The consequences of changing the relative values of the two symmetric top correlation times, which are expressed as τ_z/τ_x , on nuclear magnetic relaxation are illustrated in Figures 6 and 7. Figure 6 shows the theoretical 18.80 T T_1 values as a function of τ_x using $\beta = 60^\circ$ and three different values of τ_z/τ_x , and the corresponding η_{C} data are shown in Figure 7. In both figures, the $\tau_z/\tau_x = 1$ curve corresponds to the isotropic reorientation of the $^{13}\text{C}-^1\text{H}$ vector.

The simplest and most-straightforward approach to explaining the effects of varying τ_z/τ_x is by considering the expression in terms of an effective correlation time (not the τ_e specifically defined in eq 10). Increasing τ_z/τ_x results in a larger values for the effective correlation time (slower rotation), which will be directly reflected in the calculated relaxation times and η_{C} values. For example, Figure 6 reveals that as τ_z/τ_x values increase from 1 to 10, T_1 values decrease for all $\tau_x < 1/\omega$ (the extreme narrowing region) and increase for larger τ_x values; these are the same results observed when increasing molecular weight or decreasing temperature. The figure also shows that the isotropic rotor T_1 curve appears to be displaced horizontally toward shorter values of τ_x (faster rotation) when τ_z/τ_x is changed from 1 to 10. An analogous horizontal displacement of the isotropic rotor η_{C} curve is also shown in Figure 7 and also occurs for T_2 curves (not shown). Such displacements occur concomitantly for all relaxation times and η_{C} values, as long as τ_z/τ_x increases. However, the amount of this displacement decreases as τ_z/τ_x values increase because the same increment of τ_z contributes continually less to the value of τ_z/τ_x as it increases. And, as expected, the opposite effect occurs when the value of τ_z/τ_x is decreased. In Figures 6 and 7 for example, when τ_z/τ_x is decreased from 1 to 0.1, the isotropic rotor T_1 and η_{C} curves are horizontally displaced toward larger τ_x values.

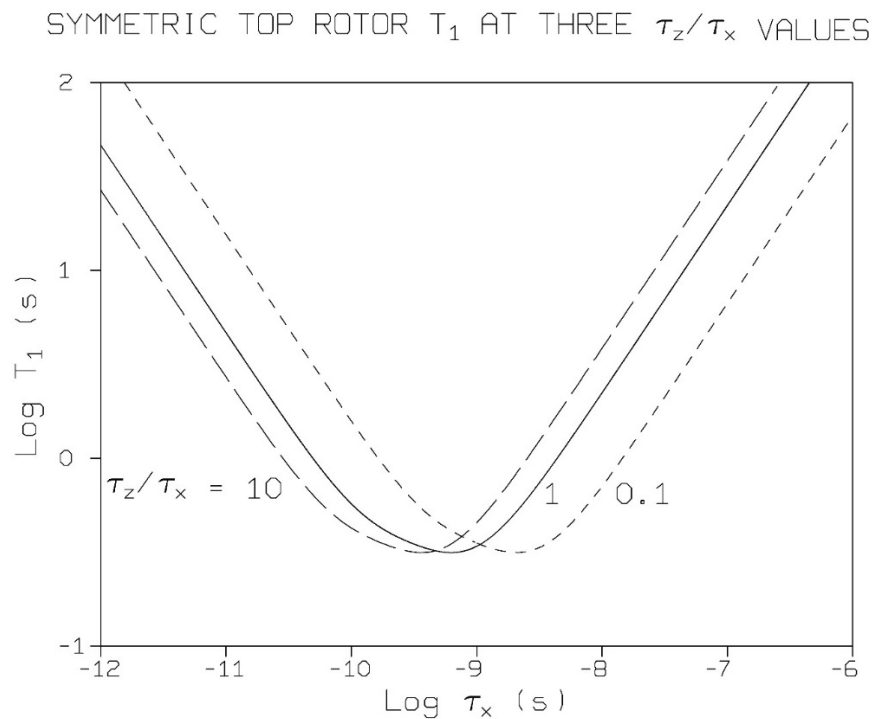


Figure 6. Rigid symmetric top rotor T_1 as a function of τ_x for different values of τ_z/τ_x . Results were calculated using $\beta = 60^\circ$; a magnetic field strength of 18.80 T; and τ_z/τ_x values of 0.1, 1, and 10.

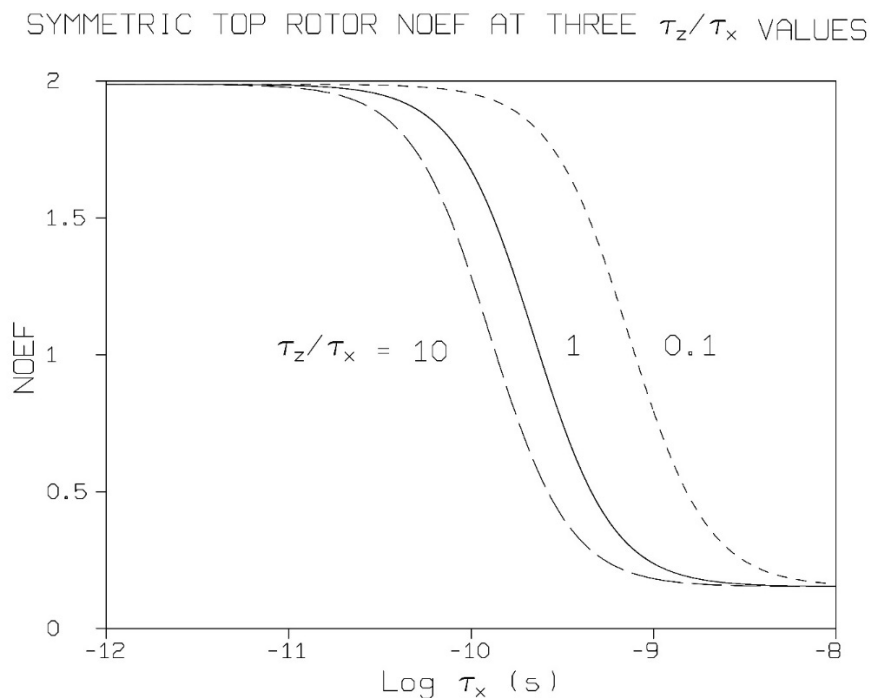


Figure 7. Rigid symmetric top rotor η_C (NOEF) as a function of τ_x for different values of τ_z/τ_x . Results were calculated using $\beta = 60^\circ$; a magnetic field strength of 18.80 T; and τ_z/τ_x values of 0.1, 1, and 10.

4.3 The Flexible Symmetric Top Rotor Model

The consequences of adding internal motion into the symmetric top rotor model are most easily demonstrated by using the τ_e that is defined in eq 10. Figure 8 shows the change in τ_e for an ellipsoid with $\tau_z/\tau_x = 3.5$ as a function of β and θ . The results clearly revealed that in the presence of such conformational motion (increasing θ), the dependence of τ_e on β diminishes. When the extent of internal conformational motion approaches 25° , the β dependence of the correlation time is somewhat diminished, and it becomes somewhat negligible at around 45° of motion. In the presence of sufficient internal motion, therefore, the strong dependence on β , shown in Figure 5, would significantly diminish, and the displacement of the T_1 curve toward longer τ_x as β increases from 0 to 90° would become more modest (not shown).

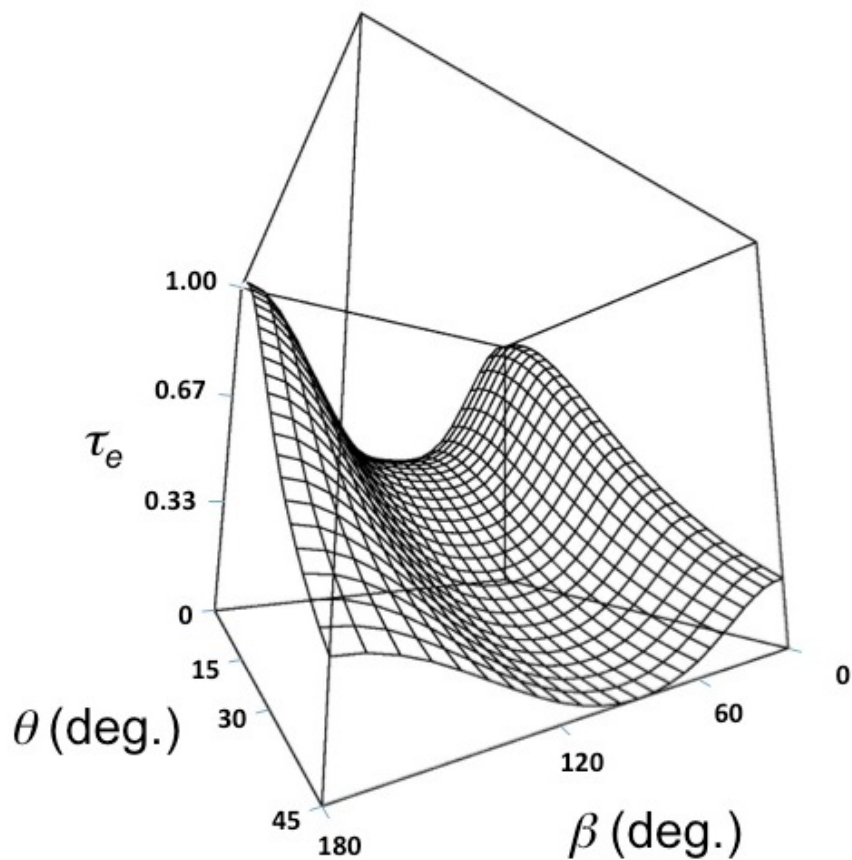


Figure 8. The diminishing dependence on β induced by increasing internal motion. The flexible symmetric top rotor τ_e is plotted as a function of β and θ for $\tau_z/\tau_x = 3.5$. Values for τ_e are relative to the highest value on the three-dimensional surface, and all angles are shown in degrees.

5. DISCUSSION AND CONCLUSIONS

A total of 25 mathematical modeling programs have been developed for the rigid isotropic and symmetric top rotor models, as well as for the flexible symmetric top rotor model. These modeling programs were used to plot the dependence of T_1 , T_2 , and η_C on various correlation times. The programs all used one of four different magnetic field strengths: 11.75, 16.45, 18.8, or 21.5 T, which are the commercially available field strengths that are commonly used for ^{13}C nuclear magnetic relaxation investigations. All programs were rigorously tested to ensure that the results returned were in agreement with the relaxation behavior that was described in the textbooks and scientific literature. Particular attention was given to those programs that used the two symmetric top rotor models, as changing their corresponding parameters to specific values must return results that are identical to the isotropic rotor or rigid symmetric top models. For example, Figure 5 shows that the rigid symmetric top rotor model returned the rigid isotropic rotor model at $\beta = 0^\circ$, and Figures 6 and 7 showed this same effect when $\tau_z/\tau_x = 1$. In a similar manner, the flexible symmetric top rotor model was tested for its ability to return the rigid symmetric top rotor model by removing all internal motion. The end result is very robust computer code that can be used for modeling ^{13}C nuclear magnetic relaxation data in terms of the three models studied herein. One useful modification of the programs would be to keep the robust mathematical code unaltered while adding new code statements that would allow experimental relaxation data to be curve-fit to each of the models (Henderson et al., 2003). Such modifications are currently in progress, along with the creation of additional mathematical modeling programs that use statistical distributions of correlation times to model very flexible molecules (McCall et al., 1959; Connor, 1964; Schaefer, 1973).

LITERATURE CITED

- Connor, T.M. Distributions of Correlation Times and Their Effect on the Comparison of Molecular Motions Derived from Nuclear Spin-Lattice and Dielectric Relaxation. *Trans. Faraday Soc.* **1964**, *60*, 1574–1591.
- Doddrell, D.; Glushko, V.; Allerhand, A. Theory of Nuclear Overhauser Enhancement and ^{13}C - ^1H Dipolar Relaxation in Proton-Decoupled Carbon-13 NMR Spectra of Macromolecules. *J. Chem. Phys.* **1972**, *56*, 3683–3689.
- Farrar, T.C.; Becker, E.D. *Pulse and Fourier Transform NMR: An Introduction to Theory and Methods*; Academic Press, Inc.: New York, 1971.
- Fukushima, E.; Roeder, S.B.W. *Experimental Pulse NMR: A Nuts and Bolts Approach*; Addison-Wesley Publishing: Reading, MA, 1981.
- Harris, R.K. *Nuclear Magnetic Resonance Spectroscopy*; Longman Publishing Group: London, 1986.
- Heatley, F. Nuclear Magnetic Relaxation of Synthetic Polymers in Dilute Solution. *Prog. Nucl. Magn. Reson. Spectrosc.* **1979**, *13*, 47–85.
- Henderson, T.J.; Venable, R.M.; Egan, W. Conformational Flexibility of the Group B Meningococcal Polysaccharide in Solution. *J. Am. Chem. Soc.* **2003**, *125* (10), 2930–2939.
- Lyerla, J.R., Jr.; Levy, G.C. Carbon-13 Nuclear Spin Relaxation. In *Topics in Carbon-13 NMR Spectroscopy*; Levy, G.C., Ed.; Wiley: New York, 1974, Vol. 1, p 81.
- McCall, D.W.; Douglass, D.C.; Anderson, E.W. Molecular Motion in Polyethylene. 2. *J. Chem. Phys.* **1959**, *30* (5), 1272–1275.
- Schaefer, J. Distributions of Correlation Times and the Carbon-13 Nuclear Magnetic Resonance Spectra of Polymers. *Macromolecules* **1973**, *6*, 882–888.
- Schleich, T.; Morgan, C.F.; Caines, G.H. Protein Rotational Correlation Times by Carbon-13 Rotating-Frame Spin-Lattice Relaxation in the Presence of Off-Resonance Radiofrequency Field. *Methods Enzymol.* **1989**, *176*, 386–418.
- Torchia, D.A.; Lyerla, J.R.; Quattrone, A.J. Molecular Dynamics and Structure of the Random Coil and Helical States of the Collagen Peptide, $\alpha 1$ -CB2, as Determined by ^{13}C Magnetic Resonance. *Biochemistry* **1975**, *14* (5), 887–900.

Withka, J.M.; Swaminathan, S.; Bolton, P.H. A Critique of the Interpretation of Nuclear Overhauser Effects of Duplex DNA. In *Computational Aspects of the Study of Biological Macromolecules by Nuclear Magnetic Resonance Spectroscopy*; Hoch, J.C., Ed.; Plenum Press: New York, 1991; Vol. 225, pp 409–420.

Woessner, D.E. Nuclear Spin Relaxation in Ellipsoids Undergoing Rotational Brownian Motion. *J. Chem. Phys.* **1962**, 37 (3), 647–654.

ACRONYMS AND ABBREVIATIONS

β	angle between the ^{13}C - ^1H bond (^{13}C - ^1H relaxation vector) and the prolate ellipsoid major (z) axis in a symmetric top rotor
γ_{C}	magnetogyric ratio for ^{13}C nuclei
γ_{H}	magnetogyric ratio for protons
ε	square root of the mean square azimuthal angle of motion for a flexible symmetric top rotor
θ	square root of the mean square polar angle of motion for a flexible symmetric top rotor
μ_0	permeability of free space
ρ	angle between the ^{13}C - ^1H bond (^{13}C - ^1H relaxation vector) and the direction of a static magnetic field (the z axis of a Cartesian coordinate system fixed in the laboratory frame)
τ_{c}	isotropic rotational correlation time
τ_{e}	flexible symmetric top rotor effective correlation time
τ_x	symmetric top correlation time for rotation about the minor (x) axis
τ_z	symmetric top correlation time for rotation about the major (z) axis
ω_{C}	resonance frequency for ^{13}C nuclei
ω_{H}	resonance frequency for protons
^{13}C NMR	carbon-13 nuclear magnetic resonance
$F_n(t)$	space function for the n^{th} dimension defined in the laboratory-fixed frame
$G_n(\tau)$	autocorrelation function for all time-dependent motional events in the n^{th} dimension, defined in the laboratory-fixed frame
$J(\omega)$	spectral density function
NMR	nuclear magnetic resonance
NOE	nuclear Overhauser effect
NOEF	nuclear Overhauser effect enhancement factor (also η_{C})
r_{CH}	^{13}C - ^1H internuclear distance
S^{d}	^{13}C signal integrated intensity acquired with proton irradiation
S^0	^{13}C signal integrated intensity acquired without proton irradiation
t	time
T	Tesla (unit of magnetic field strength)
T_1	spin-lattice relaxation time
T_2	spin-spin relaxation time

Blank

APPENDIX

MLAB CODE USED TO GENERATE FIGURES 2 THROUGH 8

A.1 PROGRAM CODE FOR FIGURE 2

```
"ISOPLOTT1.DO:  A MLAB program which plots {1H}13C T1 values as a function of      "
"               correlation time for a rigid isotropic rotor                        "
"                                                                                   "
"               Code for 16.45, 18.80 and 21.15 T static fields                    "
"                                                                                   "
"               WRITTEN 30-31 OCTOBER 2013 BY TERRY J. HENDERSON                  "
"                                                                                   "

/*               PLOT WINDOW STATEMENTS                                           */

DELETE W
WINDOW -12 TO -6, -1 TO 2 IN W
XAXIS -12:-6:1&'-1 PT DTICK LABEL -12:-6:1 LABELSIZE .015 FFRACT OFFSET(-.02, -.03) IN W
YAXIS -12&'-1:2:1 PT LTICK LABEL -1:2:1 LABELSIZE .015 FFRACT OFFSET(-.04, -.007) IN W
TITLE "ISOTROPIC ROTOR T'.3D'.7S1'1.43S'.3U" AT (.31,.9)FFRACT IN W
TITLE "21.15 T" AT (.6,.8)FFRACT IN W
TITLE "16.45 T and" AT (.57,.25)FFRACT IN W
TITLE "18.80 T (center)" AT (.525,.2)FFRACT IN W
TITLE "Log '15Tt'R'.3D'.7sc'1.43s'.3U (s)" AT (.41, 0.04) FFRACT IN W
TITLE "Log T'.3D'.7S1'1.435S'.3U (s)" AT (.06,.38) FFRACT ANGLE 90 IN W

/*               SPECTRAL DENSITY FUNCTIONS                                       */

/*               For 16.45 T - 700 MHz Operating Frequency                         */

FUNCTION CAR7(TAU) = (2*TAU)/(1+((1.22367*10^18)*((TAU)^2)))
FUNCTION DIF7(TAU) = (2*TAU)/(1+((1.08431*10^19)*((TAU)^2)))
FUNCTION SUM7(TAU) = (2*TAU)/(1+((3.03079*10^19)*((TAU)^2)))

/*               For 18.80 T - 800 MHz Operating Frequency                         */

FUNCTION CAR8(TAU) = (2*TAU)/(1+((1.59829*10^18)*((TAU)^2)))
FUNCTION DIF8(TAU) = (2*TAU)/(1+((1.41614*10^19)*((TAU)^2)))
FUNCTION SUM8(TAU) = (2*TAU)/(1+((3.95845*10^19)*((TAU)^2)))

/*               For 21.15 T - 900 MHz Operating Frequency                         */

FUNCTION CAR9(TAU) = (2*TAU)/(1+((2.023*10^18)*((TAU)^2)))
FUNCTION DIF9(TAU) = (2*TAU)/(1+((1.79226*10^19)*((TAU)^2)))
FUNCTION SUM9(TAU) = (2*TAU)/(1+((5.01002*10^19)*((TAU)^2)))

/*               EXPRESSIONS FOR T1                                              */

/*               For 16.45 T - 700 MHz Operating Frequency                         */

FUNCTION T1L(TAU) = (9.30908*10^-10)/(DIF7(TAU)+(3*CAR7(TAU))+(6*SUM7(TAU)))

/*               For 18.80 T - 800 MHz Operating Frequency                         */

FUNCTION T1M(TAU) = (9.30908*10^-10)/(DIF8(TAU)+(3*CAR8(TAU))+(6*SUM8(TAU)))

/*               For 21.15 T - 900 MHz Operating Frequency                         */

FUNCTION T1H(TAU) = (9.30908*10^-10)/(DIF9(TAU)+(3*CAR9(TAU))+(6*SUM9(TAU)))

/*               OUTPUT STATEMENTS                                               */

/*               For 16.45 T                                                      */

P1 = POINTS(T1L, 1E-12:1E-9:1E-14)
P2 = POINTS(T1L, 1E-9:1E-6:1E-11)
```

```

DRAW LOGLOG(P1)
DRAW LOGLOG(P2)

/*                                     For 18.80 T                                     */

U1 = POINTS(T1M, 1E-12:1E-9:1E-14)
U2 = POINTS(T1M, 1E-9:1E-6:1E-11)
DRAW LOGLOG(U1) LT 2
DRAW LOGLOG(U2) LT 2

/*                                     For 21.15 T                                     */

X1 = POINTS(T1H, 1E-12:1E-9:1E-14)
X2 = POINTS(T1H, 1E-9:1E-6:1E-11)
DRAW LOGLOG(X1) LT 3
DRAW LOGLOG(X2) LT 3

VIEW

```

A.2 PROGRAM CODE FOR FIGURE 3

```

"ISOPLOTT2.DO: A MLAB program which plots {1H}13C T2 values as a function of      "
"               correlation time for a rigid isotropic rotor                       "
"                                                                                   "
"               Code for 16.45, 18.80 and 21.15 T static fields                   "
"                                                                                   "
"               WRITTEN 30-31 OCTOBER 2013 BY TERRY J. HENDERSON                 "
"                                                                                   "

/*                                     PLOT WINDOW STATEMENTS                       */

DELETE W
WINDOW -12 TO -6, -4 TO 2 IN W
XAXIS -12:-6:1&'-4 PT DTICK LABEL -12:-6:1 LABELSIZE .015 FFRACT OFFSET(-.02, -.03) IN W
YAXIS -12&' -4:2:1 PT LTICK LABEL -4:2:1 LABELSIZE .015 FFRACT OFFSET(-.04, -.007) IN W
TITLE "ISOTROPIC ROTOR T'.3D'.7S2'1.435S'.3U" AT (.31,.9)FFRACT IN W
TITLE "21.15 T" AT (.42,.6) IN W
TITLE "16.45 T and" AT (.28,.47) IN W
TITLE "18.80 T (center)" AT (.23,.42) IN W
TITLE "Log '15Tt'R'.3D'.7sc'1.43s'.3U (s)" AT (.41, 0.04) FFRACT IN W
TITLE "Log T'.3D'.7S2'1.435S'.3U (s)" AT (.06,.38) FFRACT ANGLE 90 IN W

/*                                     SPECTRAL DENSITY FUNCTIONS                   */

/*               Zero-Frequency Spectral Density (independent of magnetic field strength) */

FUNCTION ZER(TAU) = 2*TAU

/*Spectral Densities for Protons, Carbon-13 Nuclei, and Both the Sum and Difference Frequencies*/
/*               (all dependent on magnetic field strength)                       */

/*               For 16.45 T - 700 MHz Operating Frequency                       */

FUNCTION CAR7(TAU) = (2*TAU)/(1+((1.22367*10^18)*((TAU)^2)))
FUNCTION PRO7(TAU) = (2*TAU)/(1+((1.93518*10^19)*((TAU)^2)))
FUNCTION DIF7(TAU) = (2*TAU)/(1+((1.08431*10^19)*((TAU)^2)))
FUNCTION SUM7(TAU) = (2*TAU)/(1+((3.03079*10^19)*((TAU)^2)))

/*               For 18.80 T - 800 MHz Operating Frequency                       */

FUNCTION CAR8(TAU) = (2*TAU)/(1+((1.59829*10^18)*((TAU)^2)))
FUNCTION PRO8(TAU) = (2*TAU)/(1+((2.52746*10^19)*((TAU)^2)))
FUNCTION DIF8(TAU) = (2*TAU)/(1+((1.41614*10^19)*((TAU)^2)))
FUNCTION SUM8(TAU) = (2*TAU)/(1+((3.95845*10^19)*((TAU)^2)))

/*               For 21.15 T - 900 MHz Operating Frequency                       */

FUNCTION CAR9(TAU) = (2*TAU)/(1+((2.023*10^18)*((TAU)^2)))

```

```

FUNCTION PRO9(TAU) = (2*TAU)/(1+((3.19884*10^19)*((TAU)^2)))
FUNCTION DIF9(TAU) = (2*TAU)/(1+((1.79226*10^19)*((TAU)^2)))
FUNCTION SUM9(TAU) = (2*TAU)/(1+((5.01002*10^19)*((TAU)^2)))

/*
                                EXPRESSIONS FOR T2
*/
/*
                                For 16.45 T - 700 MHz Operating Frequency
*/
FUNCTION T2L(TAU) = (1.86182*10^-
9)/((4*ZER(TAU))+DIF7(TAU)+(3*CAR7(TAU))+(6*PRO7(TAU))+(6*SUN7(TAU)))
/*
                                For 18.80 T - 800 MHz Operating Frequency
*/
FUNCTION T2M(TAU) = (1.86182*10^-
9)/((4*ZER(TAU))+DIF8(TAU)+(3*CAR8(TAU))+(6*PRO8(TAU))+(6*SUN8(TAU)))
/*
                                For 21.15 T - 900 MHz Operating Frequency
*/
FUNCTION T2H(TAU) = (1.86182*10^-
9)/((4*ZER(TAU))+DIF9(TAU)+(3*CAR9(TAU))+(6*PRO9(TAU))+(6*SUN9(TAU)))

/*
                                OUTPUT STATEMENTS
*/
/*
                                For 16.45 T
*/
Q1 = POINTS(T2L, 1E-12:1E-9:1E-14)
Q2 = POINTS(T2L, 1E-9:1E-6:1E-11)
DRAW LOGLOG(Q1)
DRAW LOGLOG(Q2)

/*
                                For 18.80 T
*/
V1 = POINTS(T2M, 1E-12:1E-9:1E-14)
V2 = POINTS(T2M, 1E-9:1E-6:1E-11)
DRAW LOGLOG(V1) LT 2
DRAW LOGLOG(V2) LT 2

/*
                                For 21.15 T
*/
Y1 = POINTS(T2H, 1E-12:1E-9:1E-14)
Y2 = POINTS(T2H, 1E-9:1E-6:1E-11)
DRAW LOGLOG(Y1) LT 3
DRAW LOGLOG(Y2) LT 3

VIEW

```

A.3 PROGRAM CODE FOR FIGURE 4

```

"ISOPLOTNOE.DO:  MLAB program which plots {1H}13C NOEF values as a function of      "
"                  correlation time for a rigid isotropic rotor                      "
"                                                                                   "
"                  Code for 16.45, 18.80 and 21.15 T static fields                  "
"                                                                                   "
"                  WRITTEN 30-31 OCTOBER 2013 BY TERRY J. HENDERSON                "
"                                                                                   "

/*                                                                                   */
                                PLOT WINDOW STATEMENTS
/*

DELETE W
WINDOW -11 TO -8, 0 TO 2.5 IN W
XAXIS -11:-8:1&'0 PT DTICK LABEL -11:-8:1 LABELSIZE .015 FFRACT OFFSET(-.02, -.03) IN W
YAXIS -11&'0:2.5:.5 PT LTICK LABEL 0:2.5:.5 LABELSIZE .015 FFRACT OFFSET(-.06, -.007) IN W
TITLE "ISOTROPIC ROTOR NOEF" AT (.30,.9)FFRACT IN W
TITLE "18.8 T (center)" AT (.15,.4)FFRACT IN W
TITLE "and 21.15 T" at (.18,.35)FFRACT IN W
TITLE "16.45 T" AT (.4,.65)FFRACT IN W
TITLE "Log '15Tt'R'.3D'.7sc'.1.43s'.3U (s)" AT (.41, 0.04) FFRACT IN W
TITLE "NOEF" AT (.055,.449) FFRACT ANGLE 90 IN W

/*                                                                                   */
                                SPECTRAL DENSITY FUNCTIONS
/*
                                For 16.45 T - 700 MHz Operating Frequency
/*
FUNCTION CAR7(TAU) = (2*TAU)/(1+((1.22367*10^18)*((TAU)^2)))
FUNCTION DIF7(TAU) = (2*TAU)/(1+((1.08431*10^19)*((TAU)^2)))
FUNCTION SUM7(TAU) = (2*TAU)/(1+((3.03079*10^19)*((TAU)^2)))

/*
                                For 18.80 T - 800 MHz Operating Frequency
/*
FUNCTION CAR8(TAU) = (2*TAU)/(1+((1.59829*10^18)*((TAU)^2)))
FUNCTION DIF8(TAU) = (2*TAU)/(1+((1.41614*10^19)*((TAU)^2)))
FUNCTION SUM8(TAU) = (2*TAU)/(1+((3.95845*10^19)*((TAU)^2)))

/*
                                For 21.15 T - 900 MHz Operating Frequency
/*
FUNCTION CAR9(TAU) = (2*TAU)/(1+((2.023*10^18)*((TAU)^2)))
FUNCTION DIF9(TAU) = (2*TAU)/(1+((1.79226*10^19)*((TAU)^2)))
FUNCTION SUM9(TAU) = (2*TAU)/(1+((5.01002*10^19)*((TAU)^2)))

/*                                                                                   */
                                EXPRESSIONS FOR NOEF
/*
                                For 16.45 T - 700 MHz Operating Frequency
/*
FUNCTION NOEFL(TAU) = 3.97607*(((6*SUM7(TAU))-DIF7(TAU))/(DIF7(TAU)+(3*CAR7(TAU))+(6*SUM7(TAU))))

/*
                                For 18.80 T - 800 MHz Operating Frequency
/*
FUNCTION NOEFM(TAU) = 3.97607*(((6*SUM8(TAU))-DIF8(TAU))/(DIF8(TAU)+(3*CAR8(TAU))+(6*SUM8(TAU))))

/*
                                For 21.15 T - 900 MHz Operating Frequency
/*
FUNCTION NOEFH(TAU) = 3.97607*(((6*SUM9(TAU))-DIF9(TAU))/(DIF9(TAU)+(3*CAR9(TAU))+(6*SUM9(TAU))))

/*                                                                                   */
                                OUTPUT STATEMENTS
/*
                                For 16.45 T
/*
R1 = POINTS(NOEFL, 1E-12:1E-9:1E-14)
R2 = POINTS(NOEFL, 1E-9:1E-6:1E-11)
DRAW LOGLIN(R1)
DRAW LOGLIN(R2)

/*
                                For 18.80 T
/*
W1 = POINTS(NOEFM, 1E-12:1E-9:1E-14)
W2 = POINTS(NOEFM, 1E-9:1E-6:1E-11)

```

```

DRAW LOGLIN(W1) LT 2
DRAW LOGLIN(W2) LT 2

/*
For 21.15 T
*/

Z1 = POINTS(NOEFH, 1E-12:1E-9:1E-14)
Z2 = POINTS(NOEFH, 1E-9:1E-6:1E-11)
DRAW LOGLIN(Z1) LT 3
DRAW LOGLIN(Z2) LT 3

```

```
VIEW
```

A.4 PROGRAM CODE FOR FIGURE 5

```

"SYMMTOPPLOTT1BYBETA.DO: A MLAB program that plots {1H}13C T1 values as a function of
" correlation times for rigid symmetric top rotors with a tau-x
" three-times larger than Tz and beta values of 0, 30, 60 and 90 degrees"
"
" Code is for a 18.80 T static field (800 MHz operating frequency)
"
" WRITTEN 01 - 02 MAY 2014 BY TERRY J. HENDERSON
"

/*
PLOT WINDOW STATEMENTS
*/

DELETE W
WINDOW -12 TO -6, -1 TO 2 IN W
XAXIS -12:-6:1&'-1 PT DTICK LABEL -12:-6:1 LABELSIZE .015 FFRACT OFFSET(-.02, -.03) IN W
YAXIS -12&'-1:2:1 PT LTICK LABEL -1:2:1 LABELSIZE .015 FFRACT OFFSET(-.04, -.007) IN W
TITLE "SYMMETRIC TOP ROTOR T'.3D'.7S1'1.435S'.3U FOR VARIOUS '15Tb'R' -ANGLES" AT (.08,.94)\
FFRACT IN W
TITLE "'15Tt'R'.3D'.7sz'1.43s'.3U' /'15Tt'R'.3D'.7sx'1.43s'.3U' = 8 at 18.8 Tesla" AT (.26,.81)\
FFRACT IN W
TITLE "Log '15Tt'R'.3D'.7sx'1.43s'.3U (s)" AT (.41, 0.04) FFRACT IN W
TITLE "Log T'.3D'.7S1'1.435S'.3U (s)" AT (.06,.38) FFRACT ANGLE 90 IN W

/*
TAU-X AND TAU-Z
*/

FUNCTION Tz(Tx) = (1/3)*Tx /* Tau-x is three times as long as tau-z */

/*
SPECTRAL DENSITY FUNCTIONS
*/

FUNCTION CAR8(Tx) = (2*((6*Tx)*(((.25*(((3*((COSD(B))^2))-1)^2))/6)+ \
((.75*((SIND(2*B))^2))/(5+(Tx/Tz(Tx))))+((.75*((SIND(B))^4))/(2+(4*(Tx/Tz(Tx)))))))/ \
(1+((1.59829*10^18)*(((6*Tx)*(((.25*(((3*((COSD(B))^2))-1)^2))/6)+ \
((.75*((SIND(2*B))^2))/(5+(Tx/Tz(Tx))))+((.75*((SIND(B))^4))/(2+(4*(Tx/Tz(Tx)))))) ^2)))

FUNCTION DIF8(Tx) = (2*((6*Tx)*(((.25*(((3*((COSD(B))^2))-1)^2))/6)+ \
((.75*((SIND(2*B))^2))/(5+(Tx/Tz(Tx))))+((.75*((SIND(B))^4))/(2+(4*(Tx/Tz(Tx)))))))/ \
(1+((1.41614*10^19)*(((6*Tx)*(((.25*(((3*((COSD(B))^2))-1)^2))/6)+ \
((.75*((SIND(2*B))^2))/(5+(Tx/Tz(Tx))))+((.75*((SIND(B))^4))/(2+(4*(Tx/Tz(Tx)))))) ^2)))

FUNCTION SUM8(Tx) = (2*((6*Tx)*(((.25*(((3*((COSD(B))^2))-1)^2))/6)+ \
((.75*((SIND(2*B))^2))/(5+(Tx/Tz(Tx))))+((.75*((SIND(B))^4))/(2+(4*(Tx/Tz(Tx)))))))/ \
(1+((3.95845*10^19)*(((6*Tx)*(((.25*(((3*((COSD(B))^2))-1)^2))/6)+ \
((.75*((SIND(2*B))^2))/(5+(Tx/Tz(Tx))))+((.75*((SIND(B))^4))/(2+(4*(Tx/Tz(Tx)))))) ^2)))

/*
EXPRESSIONS FOR T1
*/

FUNCTION T1M(Tx) = (9.30908*10^-10)/(DIF8(Tx)+(3*CAR8(Tx))+(6*SUM8(Tx)))

/*
OUTPUT STATEMENTS
*/

FOR N = 1:4 DO {
    B = ((N*30)-30)
    U1 = POINTS(T1M, 1E-12:1E-9:1E-14)

```

```

U2 = POINTS(T1M, 1E-9:1E-6:1E-11)
DRAW LOGLOG(U1) LT N
DRAW LOGLOG(U2) LT N

TYPE B

}

VIEW

```

A.5 PROGRAM CODE FOR FIGURE 6

```

"SYMMTOPPLOTNOEBYLENGTH.DO:  A MLAB program which plots {1H}13C T1 values as a function of      "
"                               correlation time for rigid symmetric top rotors with tau-z/tau-x    "
"                               ratios of 0.1, 1, and 10                                     "
"                                                                                             "
"                               Code is for a 18.80 T static field (800 MHz operating frequency)  "
"                                                                                             "
"                               WRITTEN 04-05 DECEMBER 2013 BY TERRY J. HENDERSON             "
"                                                                                             "

/*                               PLOT WINDOW STATEMENTS                                     */

DELETE W
WINDOW -12 TO -6, -1 TO 2 IN W
XAXIS -12:-6:1&'-1 PT DTICK LABEL -12:-6:1 LABELSIZE .015 FFRACT OFFSET(-.02, -.03) IN W
YAXIS -12&'-1:2:1 PT LTICK LABEL -1:2:1 LABELSIZE .015 FFRACT OFFSET(-.04, -.007) IN W
TITLE "SYMMETRIC TOP ROTOR T'.3D'.7S1'1.435S'.3U AT THREE '15Tt'R'.3D'.7sz'1.43s'.3U' \
      /'15Tt'R'.3D'.7sx'1.43s' VALUES" AT (.073,.94) FFRACT IN W
TITLE "'15Tt'R'.3D'.7sz'1.43s'.3U' /'15Tt'R'.3D'.7sx'1.43s' = 10" AT (.13,.33) FFRACT IN W
TITLE "1" AT (.57,.315) FFRACT IN W
TITLE "0.1" AT (.64,.315) FFRACT IN W
TITLE "Log '15Tt'R'.3D'.7sx'1.43s'.3U (s)" AT (.41, 0.04) FFRACT IN W
TITLE "Log T'.3D'.7S1'1.435S'.3U (s)" AT (.06,.38) FFRACT ANGLE 90 IN W

/*                               Beta Angle                                             */

B = 60                               /* Beta angle = 60 degrees */

/*                               SPECTRAL DENSITY FUNCTIONS                             */

FUNCTION CAR8(Tx) = (2*((6*Tx)*(((.25*(((3*((COSD(B))^2))-1)^2))/6)+ \
  ((.75*((SIND(2*B))^2))/(5+(Tx/Tz(Tx))))+((.75*((SIND(B))^4))/(2+(4*(Tx/Tz(Tx)))))))/ \
  (1+((1.59829*10^18)*(((6*Tx)*(((.25*(((3*((COSD(B))^2))-1)^2))/6)+ \
  ((.75*((SIND(2*B))^2))/(5+(Tx/Tz(Tx))))+((.75*((SIND(B))^4))/(2+(4*(Tx/Tz(Tx))))))^2)))

FUNCTION DIF8(Tx) = (2*((6*Tx)*(((.25*(((3*((COSD(B))^2))-1)^2))/6)+ \
  ((.75*((SIND(2*B))^2))/(5+(Tx/Tz(Tx))))+((.75*((SIND(B))^4))/(2+(4*(Tx/Tz(Tx)))))))/ \
  (1+((1.41614*10^19)*(((6*Tx)*(((.25*(((3*((COSD(B))^2))-1)^2))/6)+ \
  ((.75*((SIND(2*B))^2))/(5+(Tx/Tz(Tx))))+((.75*((SIND(B))^4))/(2+(4*(Tx/Tz(Tx))))))^2)))

FUNCTION SUM8(Tx) = (2*((6*Tx)*(((.25*(((3*((COSD(B))^2))-1)^2))/6)+ \
  ((.75*((SIND(2*B))^2))/(5+(Tx/Tz(Tx))))+((.75*((SIND(B))^4))/(2+(4*(Tx/Tz(Tx)))))))/ \
  (1+((3.95845*10^19)*(((6*Tx)*(((.25*(((3*((COSD(B))^2))-1)^2))/6)+ \
  ((.75*((SIND(2*B))^2))/(5+(Tx/Tz(Tx))))+((.75*((SIND(B))^4))/(2+(4*(Tx/Tz(Tx))))))^2)))

/*                               EXPRESSIONS FOR T1                                     */

FUNCTION T1M(Tx) = (9.30908*10^-10)/(DIF8(Tx)+(3*CAR8(Tx))+(6*SUM8(Tx)))

/*                               OUTPUT STATEMENTS                                     */

FUNCTION Tz(Tx) = Tx
U1 = POINTS(T1M, 1E-12:1E-9:1E-14)

```

```

U2 = POINTS(T1M, 1E-9:1E-6:1E-11)
DRAW LOGLOG(U1) LT 1
DRAW LOGLOG(U2) LT 1

```

```

FUNCTION Tz(Tx) = 0.1*Tx
  U1 = POINTS(T1M, 1E-12:1E-9:1E-14)
  U2 = POINTS(T1M, 1E-9:1E-6:1E-11)
  DRAW LOGLOG(U1) LT 2
  DRAW LOGLOG(U2) LT 2

```

```

FUNCTION Tz(Tx) = 10*Tx
  U1 = POINTS(T1M, 1E-12:1E-9:1E-14)
  U2 = POINTS(T1M, 1E-9:1E-6:1E-11)
  DRAW LOGLOG(U1) LT 3
  DRAW LOGLOG(U2) LT 3

```

VIEW

A.6 PROGRAM CODE FOR FIGURE 7

```

"SYMMTOPPLOTNOEBYLENGTH.DO:  A MLAB program which plots {1H}13C NOEF values as a function of "
"                               correlation time for rigid symmetric top rotors with tau-z/tau-x "
"                               ratios of 0.1, 1, and 10 "
"                               "
"                               Code is for a 18.80 T static field (800 MHz operating frequency "
"                               "
"                               WRITTEN 05 DECEMBER 2013 BY TERRY J. HENDERSON "
"                               "

/*                               PLOT WINDOW STATEMENTS                               */

DELETE W
WINDOW -12 TO -8, 0 TO 2 IN W
XAXIS -12:-8:1&'0 PT DTICK LABEL -12:-8:1 LABELSIZE .015 FFRACT OFFSET(-.02, -.03) IN W
YAXIS -12&'0:2:.5 PT LTICK LABEL 0:2:.5 LABELSIZE .015 FFRACT OFFSET(-.06, -.007) IN W
TITLE "SYMMETRIC TOP ROTOR NOEF AT THREE '15Tt'R'.3D'.7sz'1.43s'.3U' \
      /'15Tt'R'.3D'.7sx'1.43s' VALUES" AT (.045,.94) FFRACT IN W
TITLE "'15Tt'R'.3D'.7sz'1.43s'.3U' /'15Tt'R'.3D'.7sx'1.43s' = 10" AT (.3,.5) FFRACT IN W
TITLE "1" AT (.6,.5) FFRACT IN W
TITLE "0.1" AT (.7,.5) FFRACT IN W
TITLE "Log '15Tt'R'.3D'.7sz'1.43s'.3U (s)" AT (.41, 0.04) FFRACT IN W
TITLE "NOEF" AT (.05,.449) FFRACT ANGLE 90 IN W

/*                               Beta Angle                               */

B = 60                               /* Beta angle = 60 degrees */

/*                               SPECTRAL DENSITY FUNCTIONS                               */

FUNCTION CAR8(Tx) = (2*((6*Tx)*(((.25*(((3*((COSD(B))^2))-1)^2))/6)+ \
  ((.75*((SIND(2*B))^2))/(5+(Tx/Tz(Tx))))+((.75*((SIND(B))^4))/(2+(4*(Tx/Tz(Tx)))))))/ \
  (1+((1.59829*10^18)*(((6*Tx)*(((.25*(((3*((COSD(B))^2))-1)^2))/6)+ \
  ((.75*((SIND(2*B))^2))/(5+(Tx/Tz(Tx))))+((.75*((SIND(B))^4))/(2+(4*(Tx/Tz(Tx))))))^2)))

FUNCTION DIF8(Tx) = (2*((6*Tx)*(((.25*(((3*((COSD(B))^2))-1)^2))/6)+ \
  ((.75*((SIND(2*B))^2))/(5+(Tx/Tz(Tx))))+((.75*((SIND(B))^4))/(2+(4*(Tx/Tz(Tx)))))))/ \
  (1+((1.41614*10^19)*(((6*Tx)*(((.25*(((3*((COSD(B))^2))-1)^2))/6)+ \
  ((.75*((SIND(2*B))^2))/(5+(Tx/Tz(Tx))))+((.75*((SIND(B))^4))/(2+(4*(Tx/Tz(Tx))))))^2)))

FUNCTION SUM8(Tx) = (2*((6*Tx)*(((.25*(((3*((COSD(B))^2))-1)^2))/6)+ \
  ((.75*((SIND(2*B))^2))/(5+(Tx/Tz(Tx))))+((.75*((SIND(B))^4))/(2+(4*(Tx/Tz(Tx)))))))/ \
  (1+((3.95845*10^19)*(((6*Tx)*(((.25*(((3*((COSD(B))^2))-1)^2))/6)+ \
  ((.75*((SIND(2*B))^2))/(5+(Tx/Tz(Tx))))+((.75*((SIND(B))^4))/(2+(4*(Tx/Tz(Tx))))))^2)))

/*                               EXPRESSIONS FOR NOEF                               */

```

```

FUNCTION NOEFM(Tx) = 3.97607*((6*SUM8(Tx))-DIF8(Tx))/(DIF8(Tx)+(3*CAR8(Tx))+(6*SUM8(Tx)))

/*
                                OUTPUT STATEMENTS
*/

FUNCTION Tz(Tx) = Tx
  W1 = POINTS(NOEFM, 1E-12:1E-9:1E-14)
  W2 = POINTS(NOEFM, 1E-9:1E-6:1E-11)
  DRAW LOGLIN(W1) LT 1
  DRAW LOGLIN(W2) LT 1

FUNCTION Tz(Tx) = 0.1*Tx
  W1 = POINTS(NOEFM, 1E-12:1E-9:1E-14)
  W2 = POINTS(NOEFM, 1E-9:1E-6:1E-11)
  DRAW LOGLIN(W1) LT 2
  DRAW LOGLIN(W2) LT 2

FUNCTION Tz(Tx) = 10*Tx
  W1 = POINTS(NOEFM, 1E-12:1E-9:1E-14)
  W2 = POINTS(NOEFM, 1E-9:1E-6:1E-11)
  DRAW LOGLIN(W1) LT 3
  DRAW LOGLIN(W2) LT 3

VIEW

```

A.7 PROGRAM CODE FOR FIGURE 8

```

"TAUEFFNET.DO: A MLAB program that plots the flexible symmetric top rotor effective correlation"
"               time as a function of beta-angle and polar angle of motion, theta
"
"               no azimuthal motion
"
"               Dz is 3.5-times larger than Dx
"
"               WRITTEN AND TESTED 7-8 MAY 2015 BY TERRY J. HENDERSON
"

DELETE w3

/*
  Polar and Azimuthal Angles of Motion, Beta Angle, and Correlation Times
*/

B = 0
/* Beta angle starts at zero degrees */

Th = 0
/* Polar angle of motion starts at 0 degrees */

Ep = 0
/* Azimuthal angle of motion is 0 degrees */

Tz = 1

FUNCTION Tx(Tz) = 3.5*Tz
/* Gives Dz/Dx = 3.5 */

/* Flexible Symmetric Top Rotor Effective Correlation Time as a Function of Beta and Theta */

FUNCTION Teff(Th, B) = (((1/4)+(9/(8*(exp(4*(Th^2)))))+(3*(cosd(2*B))/(2*(exp(2*(Th^2))))+(\
  9*(cosd(4*B))/(8*(exp(4*(Th^2)))))/(4*(Tx(Tz)^-1)))+(9*(1+(1/(2*(exp(4\
  *(Th^2)))))-(2*(cosd(2*B))/(exp(2*(Th^2))))+(\cosd(4*B))*exp((-4*(Th^2))\
  -(4*(Ep^2))))/2))/16*((Tx(Tz)^-1)+(2*(Tz^-1)))+(9*(exp(-4*(Th^2)))-(\
  exp((-4*(Th^2))-(Ep^2))*cosd(4*B)))/(4*((5*(Tx(Tz)^-1)+(Tz^-1))))

/*
                                Output Statements
*/

M = CROSS(0:0.7854:0.03272, 0:180:7.5)
/*Theta in radians, beta in degrees*/

M COL 3 = Teff on M

DRAW M LT NET

CMD3D ("BOX")
CMD3D ("TURN -55")
CMD3D ("TWIST -13")

```

```
CMD3D ("RAISE -.55")  
CMD3D ("TRACK")  
CMD3D ("DOLLY 0.4")  
CMD3D ("BOTNETCOLOR 0")
```

```
VIEW
```

Blank

DISTRIBUTION LIST

The following individuals and organizations were provided with one Adobe portable document format (pdf) electronic version of this report:

U.S. Army Edgewood Chemical
Biological Center (ECBC)
RDCB-DRC-C
ATTN: Henderson, T.
McMahon, L.

Defense Threat Reduction Agency
J9-CBS
ATTN: Graziano, A.

Department of Homeland Security
RDCB-PI-CSAC
ATTN: Negron, A.
DHS-S&T-RDP-CSAC
ATTN: Strang, P.

Defense Technical Information Center
ATTN: DTIC OA

G-3 History Office
U.S. Army RDECOM
ATTN: Smart, J.

ECBC Technical Library
RDCB-DRB-BL
ATTN: Foppiano, S.
Stein, J.

Office of the Chief Counsel
AMSRD-CC
ATTN: Upchurch, V.

ECBC Rock Island
RDCB-DES
ATTN: Lee, K.
RDCB-DEM
ATTN: Grodecki, J.

